Available online at www.sciencedirect.com
SCIENCE DIRECT®
International Journal of Thermal Sciences 45 (2006) 41–50
International Journal of Thermal Sciences
www.elsevier.com/locate/ijts

Analytical modelling of temperature distribution in resistive thin-film thermal sensors

Alexander G. Kozlov *

Omsk Branch of Institute of Semiconductor Physics, Russian Academy of Sciences, Siberian Branch, Pr. Mira, 55a, Omsk 644077, Russia

Received 1 October 2004; received in revised form 28 April 2005; accepted 28 April 2005

Available online 6 June 2005

Abstract

The method of modelling the temperature distribution in resistive thin-film thermal sensors is presented. This method is based upon the division of the sensor into the unit subdomains whose structure is substituted by an equivalent structure. In its turn, the equivalent structure of the unit subdomain is divided into four rectangular regions. For each region, the analytical expression of the temperature distribution is determined using the Fourier method. In addition, each heat flux density between the adjacent regions and between the regions and the ambient air is defined as the sum of orthogonal functions with unknown weighting coefficients. To find the unknown weighting coefficients the adjoint boundary conditions on the boundaries between the adjacent regions and the Newton boundary conditions on the boundaries between the regions and the ambient air are used. In general, the determination of the weighting coefficients is reduced to solving a system of linear equations. The present method is used to determine the temperature distribution in the realistic resistive thin-film thermal sensor and the dependencies of the overheating temperature in the centre of meander strips of this sensor on a number of the parameters: the measuring current, the thermal conductivity and the thickness of the substrate, the convective heat transfer coefficient, the surface temperature of an object under investigation, the width of the meander strip, and the distance between meander strips.

Keywords: Analytical modelling; Fourier method; Meander structure; Resistive thin-film thermal sensor; Temperature distribution

1. Introduction

Resistive thermal sensors are widely used for measuring a temperature of various objects [1–3]. The operation principle of the sensors is founded on the dependence of the resistivity of some materials on the temperature. Among these, the sensors based on pure metals or alloys have the highest accuracy in measuring a temperature. The temperature dependence of their resistance is approximated by the following linear function

$$R = R_0\big[1 + \alpha(T - T_0)\big] \tag{1}$$

where R and R_0 are the resistances of the sensor at the temperatures T and T_0, respectively, α is the temperature resistance coefficient of resistive material, T is the operating temperature of the sensor, $T_0 = 273.15$ K is the absolute temperature corresponding 0 °C.

The resistive thermal sensors based on pure metals or alloys are made in two design versions:

(1) bulk sensors made by winding a microwire;
(2) thin-film sensors made by a vacuum deposition of pure metals or alloys on insulated substrates.

The resistive thin-film thermal sensors are the most widely used to measure a surface temperature [2,3]. In this case, it is important that a measurement error should be as small as possible. The basic component of the measurement error is the error due to the self-heating by a measuring current. To exactly estimate this error it is necessary to know the temperature distribution in the sensor. The experimental investigation of the temperature distribution presents the difficult problem due to the small dimensions of the sensor

* Tel.: +7 3812 673381; fax: +7 3812 229763.
E-mail address: kozlov@phys.omsu.omskreg.ru (A.G. Kozlov).

1290-0729/$ – see front matter
doi:10.1016/j.ijthermalsci.2005.04.009

Nomenclature

$\mathbf{A}, \mathbf{B}, \mathbf{C}, \mathbf{D}, \mathbf{E}, \mathbf{F}$	submatrices of coefficients	
a	distance between meander strips	m
B_0	coefficient	$\mathrm{W{\cdot}m^{-2}}$
B_1	coefficient	$\mathrm{W{\cdot}m^{-2}{\cdot}K^{-1}}$
b	width of the meander strip	m
b_j	width of the region j	m
d_s	thickness of the substrate	m
d_c	thickness of the connective layer	m
h	convective heat transfer coefficient	$\mathrm{W{\cdot}m^{-2}{\cdot}K^{-1}}$
I	measuring current	A
k_f	form factor of the meander	
l_j	length of the region j	m
l_md	length of the middle line of the meander	m
$\mathbf{M}$	matrix of coefficients	
P_ts	heat power generated by the sensor	W
$q^{(j,a)}$	heat flux density between the region j and the ambient air	$\mathrm{W{\cdot}m^{-2}}$
q_sh	heat power per unit area of the sensor	$\mathrm{W{\cdot}m^{-2}}$
R	resistance of the sensor	Ω
R_0	resistance of the sensor at temperature T_0	Ω
S_ts	area of the resistive layer	$\mathrm{m^2}$
T	operating temperature of the sensor	K
T_0	absolute temperature corresponding 0 °C, $T_0 = 273.15$ K	
T_j	temperature of the region j	K
T_a	temperature of the ambient air	K
T_s	surface temperature of the object under investigation	K
ΔT	overheating temperature	K
ΔT_cm	overheating temperature in the centre of the meander strip	K
ΔT_lm	overheating temperature of the resistive layer determined from the lamped model	K
x_j, y_j	Cartesian co-ordinates of the region j	m
$\mathbf{0}$	zero submatrix or subvector	

Greek symbols

α	temperature resistance coefficient of the resistive material	$\mathrm{K^{-1}}$
$\mathbf{\Delta}$	vector or subvector of weighting coefficients	
δ	weighting coefficient	$\mathrm{K{\cdot}m^{-1}}$
λ_c	thermal conductivity of the material of the connective layer	$\mathrm{W{\cdot}m^{-1}{\cdot}K^{-1}}$
λ_j	thermal conductivity of the material of the region j	$\mathrm{W{\cdot}m^{-1}{\cdot}K^{-1}}$
λ_s	thermal conductivity of the material of the substrate	$\mathrm{W{\cdot}m^{-1}{\cdot}K^{-1}}$
$\mathbf{\Phi}$	vector or subvector of right parts	

Subscripts

j, s, t	region number
k, m	summation indices

Superscripts

(j,t)	boundary between the regions j and t
(j,a)	boundary between the region j and the ambient air

and the small difference between the sensor temperature and the surface temperature of an object under investigation. The only possible method for solving this problem is mathematical simulation.

Presently, for modelling the temperature distribution in resistive thin-film thermal sensors the following methods are used:

(1) methods based on the electro-thermal analogy;
(2) numerical methods;
(3) analytical methods.

The methods based on the electro-thermal analogy make it possible to rapidly estimate the temperature of the resistive layer but they are rough and do not allow one to determine the temperature distribution in the sensor structure [3,4].

The numerical methods (the finite-element method [5–7], the boundary-element method [8], and the finite-difference method [9]) are the most frequently used to model the temperature distribution in the thermal sensors. However, these methods have the large amount of computations and the tedious work of problem definition. Furthermore, it is difficult to use these methods in the further analytical procedures such as the analytical determination of the sensor parameters and the analytical optimization of the sensor structure.

The analytical methods have a number of the advantages over the numerical methods: smaller time of problem definition; smaller amount of computations; simpler control of simulation accuracy; use of the common mathematical software (MathCAD, Maple, MATLAB, MATHEMATICA). The simplified versions of the analytical methods are widely used by the firms producing resistive thermal sensors to estimate the measurement error of these sensors (see, for example, [10]). To apply these methods to the complicate structures of thermal sensors they must be modified. Particularly, in Refs. [11,12], the analytical method is proposed and developed which makes it possible to determine the temperature distribution in the multilayered parallelepiped structures of heat-generating devices. However, this method does not allow one to take into account the convective and radiant heat transfers and, therefore, it is not recommended for determining the temperature distribution in the resistive thin-film thermal sensors, where account must be taken of all ways of the heat transfer. In this connection, there is a need to de-

velopment of the analytical methods suitable for modelling the temperature distribution in the resistive thin-film thermal sensors.

This paper presents such a method and demonstrates its use for modelling the temperature distribution in the concrete sensor.

2. Analysis of the sensor structure

The resistive thin-film thermal sensors based on pure metals or alloys have a meander form since the surface resistivity of metal thin films is small and the form factor of the sensors exceeds 10. The top view of the sensor is shown in Fig. 1(a). When the sensor is used to measure a surface temperature, it is glued or soldered to the surface of an object. The cross view of the sensor on the surface of an object is shown in Fig. 1(b). The connective layer (glue layer or solder layer) has an influence on the temperature distribution in the sensor and this influence must be taken into account.

The analysis of the sensor structure and the modelling of the temperature distribution are based on the following assumptions that allow us to simplify the geometry of the sensor:

(1) An object under investigation is assumed to be massive in comparison with the sensor and to have the large thermal conductivity and the large heat capacity. It follows that the surface temperature of the object is independent of the thermal processes in the sensor.
(2) The lateral surfaces of the sensor structure are assumed to be adiabatic. This assumption can be based as follows. The heat spreading through the lateral surfaces is far less than the heat spreading through the upper and lower surfaces. This difference follows from the difference between their areas. The heat spreading through the lateral surfaces has the pronounced effect only on the temperature distribution in the domains near these surfaces. The dimensions of the domains are commensurable with the thickness of the sensor structure and far less than the length and the width of the structure. Therefore, in modelling, the heat spreading through the lateral surfaces cannot be taken into account.
(3) The region with the metal pads has no influence on (i) the temperature distribution in the region with the meander structure and (ii) the surface temperature of the object. This assumption is based on the assumptions (1) and (2). The pronounced interference between the regions of the sensor structure is appeared in the boundary domains whose dimensions are determined by the thickness of the sensor structure and are far less than the length and the width of the regions. Therefore, based on this assumption, one can suppose that the boundary between the regions is adiabatic.

The meander structure of the resistive thin-film thermal sensor has a number of the features. The first feature is due to the fact that, as can be seen from Fig. 1(b), the meander structure has translation symmetry in the x-direction if we do not take into account the sites where the meander has bends. It is obvious that the temperature distribution in this structure also has the translation symmetry. In this case, one can neglect the temperature distribution in the sites where the meander has bends. These bends occupy the small area in comparison with the total area of the region with the meander structure and have a negligible effect on the temperature distribution in this region. Therefore, to find the temperature distribution in the sensor it is enough to determine the temperature distribution in the unit domain of its meander structure. The unit domain with the help of which one can produce the meander structure of the sensor by means of translation is shown in Fig. 1(c).

In its turn, the unit domain marked out in the meander structure has the mirror symmetry. This feature of the unit domain allows us to consider the unit subdomain marked out from the unit domain to determine the temperature distribution in this domain. This unit subdomain is shown in Fig. 1(d).

The second feature of the resistive thin-film thermal sensor is the smaller thickness of the resistive layer in comparison with the thicknesses of the substrate and the connective layer. The thickness of the resistive layer amounts usually to some tenth fraction of micrometer or less, while the thicknesses of the substrate and the connective layer amount to some unit micrometers or more. In this connection, one cannot determine the temperature distribution in the resistive layer i.e. one can exclude this layer from the consideration. However, for operating the sensor, the resistive layer generates the heat which must be taken into account in determining the temperature distribution. To overcome the mentioned difficult we assume that instead of the resistive layer the unit subdomain has the heat-generating boundary whose heat power is equal to the heat power generated by the layer. In this case, the structure of the unit subdomain can be replaced by the simpler equivalent structure with the heat-generating boundary. This equivalent structure is shown in Fig. 1(e).

Thus, the determination of the temperature distribution in the resistive thin-film thermal sensor is reduced to the determination of the temperature distribution in the equivalent structure of the unit subdomain.

3. Temperature distribution in the equivalent structure of the unit subdomain

To determine the temperature distribution in the unit subdomain we use the method proposed in Refs. [13,14]. In this method, the 2D rectangular structure is divided into a number of the rectangular regions with a homogeneous structure and homogeneous boundary conditions. For each region, the analytical expression for the temperature distribution is de-

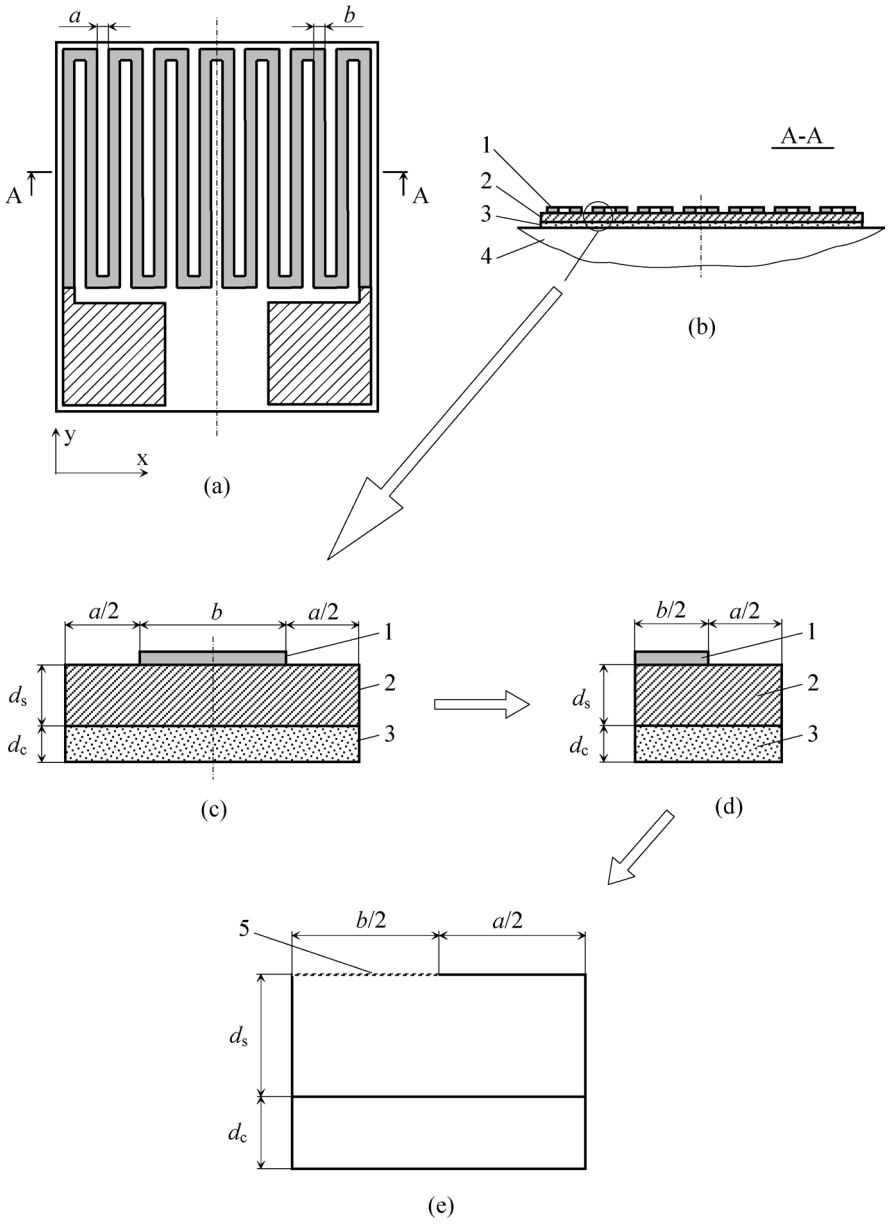

Fig. 1. Structure of the resistive thin-film thermal sensor and its unit domain and subdomain: (a) top view of the resistive thin-film thermal sensor, (b) cross view of the resistive thin-film thermal sensor, (c) cross view of the unit domain, (d) cross view of the unit subdomain, (e) equivalent structure of the unit subdomain, (1) resistive layer, (2) substrate, (3) connective layer, (4) object under investigation, (5) heat-generating boundary, (a) distance between the meander strips, (b) width of the meander strip, (d_s) thickness of the substrate, (d_c) thickness of the connective layer.

termined using the Fourier method. Each heat flux density between the adjacent regions is defined as the sum of orthogonal functions with unknown weighting coefficients. In order to find the unknown weighting coefficients the adjoint boundary conditions on the boundaries between the adjacent regions are used.

The equivalent structure of the unit subdomain has a rectangular shape and consists of two layers (the substrate and the connective layer) whose properties are different. The upper boundary of the structure is the boundary with the heterogeneous boundary conditions. The boundary has the heat-generating section. Therefore, the equivalent structure of the unit subdomain should be divided into four regions, as suggested in Fig. 2. In this case, each region has the homogeneous structure and the homogeneous boundary conditions. The dimensions of the regions are:

region 1: $l_1 = b/2$; $b_1 = d_s$;
region 2: $l_2 = a/2$; $b_2 = d_s$;
region 3: $l_3 = b/2$; $b_3 = d_c$;
region 4: $l_4 = a/2$; $b_4 = d_c$.

However, in the structure, the regions 1 and 2 have the boundaries (the upper boundary of each region) with

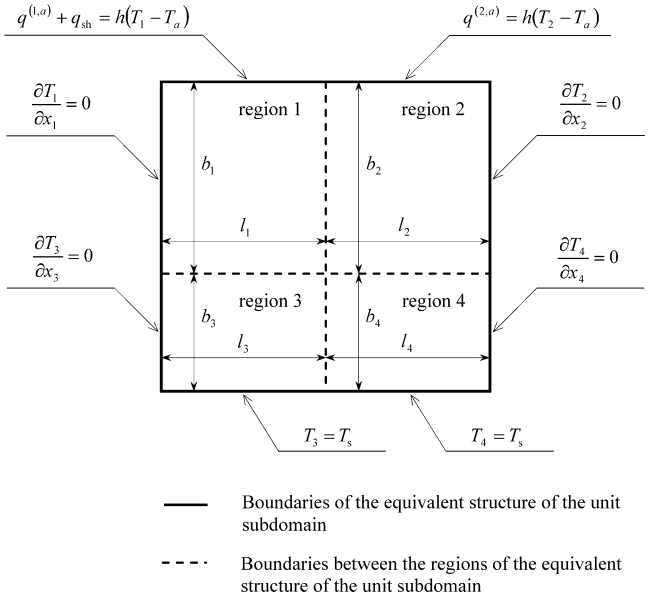

Fig. 2. Equivalent structure of the unit subdomain and its division into regions.

the Newton boundary conditions. This feature complicates the determination of the temperature distribution since the method proposed in Ref. [13] can only be used for the structures with regions having the Dirichlet and/or Neumann boundary conditions. Nevertheless, this problem can be solved, if, on the mentioned boundaries, the Neumann boundary conditions are used. Then, in the expressions for the temperature distribution in these regions, the additional unknown heat flux densities are appeared. To determine these heat flux densities through orthogonal functions with unknown weighting coefficients the Newton boundary conditions on the upper boundaries should be used.

According to Ref. [13], the temperature distribution in the four regions of the unit subdomain can be presented as follows:

$$
\begin{aligned}
T_1 = {} & \frac{-\delta_0^{(1,2)} - \delta_0^{(1,a)} + \delta_0^{(1,3)}}{l_1 b_1 \lambda_1} \\
& + \frac{2}{l_1 b_1 \lambda_1} \sum_{k=1}^{\infty} \frac{-(-1)^k \delta_0^{(1,2)} - \delta_k^{(1,a)} + \delta_k^{(1,3)}}{(k\pi/l_1)^2} \\
& \times \cos\left(\frac{k\pi x_1}{l_1}\right) \\
& + \frac{2}{l_1 b_1 \lambda_1} \sum_{m=1}^{\infty} \frac{-\delta_m^{(1,2)} - (-1)^m \delta_0^{(1,a)} + \delta_0^{(1,3)}}{(m\pi/b_1)^2} \\
& \times \cos\left(\frac{k\pi y_1}{b_1}\right) + \frac{4}{l_1 b_1 \lambda_1} \\
& \times \sum_{k=1}^{\infty} \sum_{m=1}^{\infty} \frac{-(-1)^k \delta_m^{(1,2)} - (-1)^m \delta_k^{(1,a)} + \delta_k^{(1,3)}}{(k\pi/l_1)^2 + (m\pi/b_1)^2} \\
& \times \cos\left(\frac{k\pi x_1}{l_1}\right) \cos\left(\frac{k\pi y_1}{b_1}\right)
\end{aligned} \tag{2}
$$

$$
\begin{aligned}
T_2 = {} & \frac{-\delta_0^{(2,a)} + \delta_0^{(1,2)} + \delta_0^{(2,4)}}{l_2 b_2 \lambda_2} \\
& + \frac{2}{l_2 b_2 \lambda_2} \sum_{k=1}^{\infty} \frac{-\delta_k^{(2,a)} + \delta_0^{(1,2)} + \delta_k^{(2,4)}}{(k\pi/l_2)^2} \cos\left(\frac{k\pi x_2}{l_2}\right) \\
& + \frac{2}{l_2 b_2 \lambda_2} \sum_{m=1}^{\infty} \frac{-(-1)^m \delta_0^{(2,a)} + \delta_m^{(1,2)} + \delta_0^{(2,4)}}{(m\pi/b_2)^2} \\
& \times \cos\left(\frac{k\pi y_2}{b_2}\right) \\
& + \frac{4}{l_2 b_2 \lambda_2} \sum_{k=1}^{\infty} \sum_{m=1}^{\infty} \frac{-(-1)^m \delta_k^{(2,a)} + \delta_m^{(1,2)} + \delta_k^{(2,4)}}{(k\pi/l_2)^2 + (m\pi/b_2)^2} \\
& \times \cos\left(\frac{k\pi x_2}{l_2}\right) \cos\left(\frac{k\pi y_2}{b_2}\right)
\end{aligned} \tag{3}
$$

$$
\begin{aligned}
T_3 = {} & 4T_s \sum_{m=1}^{\infty} \frac{1}{(2m-1)\pi} \sin\left[\frac{(2m-1)\pi y_3}{2b_3}\right] \\
& + \frac{2}{l_3 b_3 \lambda_3} \sum_{m=1}^{\infty} \frac{(-1)^m \delta_0^{(1,3)} - \delta_m^{(3,4)}}{[(2m-1)\pi/2b_3]^2} \\
& \times \sin\left[\frac{(2m-1)\pi y_3}{2b_3}\right] \\
& + \frac{4}{l_3 b_3 \lambda_3} \sum_{k=1}^{\infty} \sum_{m=1}^{\infty} \frac{(-1)^m \delta_k^{(1,3)} - (-1)^k \delta_m^{(3,4)}}{(k\pi/l_3)^2 + [(2m-1)\pi/2b_3]^2} \\
& \times \cos\left(\frac{k\pi x_3}{l_3}\right) \sin\left[\frac{(2m-1)\pi y_3}{2b_3}\right]
\end{aligned} \tag{4}
$$

$$
\begin{aligned}
T_4 = {} & 4T_s \sum_{m=1}^{\infty} \frac{1}{(2m-1)\pi} \sin\left[\frac{(2m-1)\pi y_4}{2b_4}\right] \\
& + \frac{2}{l_4 b_4 \lambda_4} \sum_{m=1}^{\infty} \frac{(-1)^m \delta_0^{(2,4)} + \delta_m^{(3,4)}}{[(2m-1)\pi/2b_4]^2} \\
& \times \sin\left[\frac{(2m-1)\pi y_4}{2b_4}\right] \\
& + \frac{4}{l_4 b_4 \lambda_4} \sum_{k=1}^{\infty} \sum_{m=1}^{\infty} \frac{(-1)^m \delta_k^{(2,4)} + \delta_m^{(3,4)}}{(k\pi/l_4)^2 + [(2m-1)\pi/2b_4]^2} \\
& \times \cos\left(\frac{k\pi x_4}{l_4}\right) \sin\left[\frac{(2m-1)\pi y_4}{2b_4}\right]
\end{aligned} \tag{5}
$$

where T_j is the temperature of the region j; x_j and y_j are the coordinates of the region j; l_j and b_j are the dimensions of the region j; T_s is the surface temperature of an object under investigation; λ_j is the thermal conductivity of the region j; $\lambda_1 = \lambda_2 = \lambda_s$; $\lambda_3 = \lambda_4 = \lambda_c$; λ_s and λ_c are the thermal conductivities of the substrate and the connective layer, respectively; $\delta_k^{(j,t)}$ and $\delta_m^{(j,s)}$ are the weighting coefficients defining the heat flux densities through the boundaries between the regions j and t and between the regions j and s, respectively; $\delta_k^{(j,a)}$ are the weighting coefficients defining the heat flux density through the boundary between the region j and the ambient air.

Eqs. (2)–(5) contain six types of the unknown weighting coefficients: $\delta_m^{(1,2)}$, $\delta_k^{(1,a)}$, $\delta_k^{(1,3)}$, $\delta_k^{(2,a)}$, $\delta_k^{(2,4)}$, and $\delta_m^{(3,4)}$. To

determine these coefficients one can use four temperature equality conditions on the boundaries between the adjacent regions and two Newton boundary conditions on the boundaries between the regions 1 and 2 and the ambient air. The four equations for temperature equality on the boundaries between the adjacent regions can be obtained from the following conditions:

$$T_1|_{x_1=l_1} = T_2|_{x_2=0} \tag{6}$$

$$T_1|_{y_1=0} = T_3|_{y_3=b_3} \tag{7}$$

$$T_2|_{y_2=0} = T_4|_{y_4=b_4} \tag{8}$$

$$T_3|_{x_3=l_3} = T_4|_{x_4=0} \tag{9}$$

The two equations for the Newton boundary conditions on the boundaries between the regions 1 and 2 and the ambient air should be considered in detail. The Newton boundary condition for the boundary between the region 1 and the ambient air, which is the heat-generating boundary, can be written in the following form:

$$q^{(1,a)} + q_{\mathrm{sh}} = h(T_1|_{y_1=b_1} - T_{\mathrm{a}}) \tag{10}$$

where $q^{(1,a)}$ is the heat flux density between the region 1 and the ambient air; q_{sh} is the heat power per unit area of the sensor, which is generated as a result of the self-heating by a measuring current; h is the convective heat transfer coefficient; T_{a} is the temperature of the ambient air.

The heat flux density $q^{(1,a)}$ can be determined using the equation for the heat flux density presented in Ref. [13]:

$$q^{(1,a)} = \frac{1}{l_1}\delta_0^{(1,a)} + \frac{2}{l_1}\sum_{k=1}^{\infty}\delta_k^{(1,a)}\cos\left(\frac{k\pi x_1}{l_1}\right) \tag{11}$$

The heat power per unit area of the resistive thin-film thermal sensor is given by

$$q_{\mathrm{sh}} = \frac{P_{\mathrm{ts}}}{S_{\mathrm{ts}}} \tag{12}$$

where P_{ts} is the heat power generated by the sensor; S_{ts} is the area of the resistive layer. In its turn, the parameters P_{ts} and S_{ts} are equal to

$$P_{\mathrm{ts}} = I^2R = I^2R_0\left[1 + \alpha(T_1|_{y_1=b_1} - T_0)\right] \tag{13}$$

$$S_{\mathrm{ts}} \approx l_{\mathrm{md}}b = k_{\mathrm{f}}b^2 \tag{14}$$

where I is the measuring current; l_{md} is the length of the middle line of the meander; b is the width of the meander strip; k_{f} is the form factor of the meander. In this case, the heat power per unit area of the sensor can be represented in the following form:

$$q_{\mathrm{sh}} = B_0 + B_1T_1|_{y_1=b_1} \tag{15}$$

where

$$B_0 = \frac{I^2R_0(1-\alpha T_0)}{k_{\mathrm{f}}b^2} \tag{16}$$

$$B_1 = \frac{I^2R_0\alpha}{k_{\mathrm{f}}b^2} \tag{17}$$

Using Eqs. (11) and (15) the Newton boundary condition for the boundary between the region 1 and the ambient air (Eq. (10)) can be rewritten as follows:

$$\frac{1}{l_1}\delta_0^{(1,a)} + \frac{2}{l_1}\sum_{k=1}^{\infty}\delta_k^{(1,a)}\cos\left(\frac{k\pi x_1}{l_1}\right) + B_0 + B_1T_1|_{y_1=b_1} = h(T_1|_{y_1=b_1} - T_{\mathrm{a}}) \tag{18}$$

The Newton boundary condition for the boundary between the region 2 and the ambient air can be found in the same manner as for the boundary between the region 1 and the ambient air. However, this boundary is not heat-generating and the Newton boundary condition for it has the simpler form

$$\frac{1}{l_2}\delta_0^{(2,a)} + \frac{2}{l_2}\sum_{k=1}^{\infty}\delta_k^{(2,a)}\cos\left(\frac{k\pi x_2}{l_2}\right) = h(T_2|_{y_2=b_2} - T_{\mathrm{a}}) \tag{19}$$

Inserting the expressions for the temperatures (2)–(5) in Eqs. (6)–(9), (18), and (19) yields the system of linear equations concerning the unknown weighting coefficients. It is convenient to write this system in a matrix representation

$$\mathbf{M}\boldsymbol{\Delta} = \boldsymbol{\Phi} \tag{20}$$

where $\mathbf{M}$ is the matrix of the coefficients; $\boldsymbol{\Delta}$ is the vector of the unknown weighting coefficients; $\boldsymbol{\Phi}$ is the vector of the right parts.

The matrix $\mathbf{M}$ and the vectors $\boldsymbol{\Delta}$ and $\boldsymbol{\Phi}$ have the following forms in a block matrix representation

$$\mathbf{M} = \begin{bmatrix} \mathbf{A}_m^{(1,2)} & \mathbf{A}_k^{(1,a)} & \mathbf{A}_k^{(1,3)} & \mathbf{A}_k^{(2,a)} & \mathbf{A}_k^{(2,4)} & \mathbf{0} \\ \mathbf{B}_m^{(1,2)} & \mathbf{B}_k^{(1,a)} & \mathbf{B}_k^{(1,3)} & \mathbf{0} & \mathbf{0} & \mathbf{0} \\ \mathbf{C}_m^{(1,2)} & \mathbf{C}_k^{(1,a)} & \mathbf{C}_k^{(1,3)} & \mathbf{0} & \mathbf{0} & \mathbf{C}_m^{(3,4)} \\ \mathbf{D}_m^{(1,2)} & \mathbf{0} & \mathbf{0} & \mathbf{D}_k^{(2,a)} & \mathbf{D}_k^{(2,4)} & \mathbf{0} \\ \mathbf{E}_m^{(1,2)} & \mathbf{0} & \mathbf{0} & \mathbf{E}_k^{(2,a)} & \mathbf{E}_k^{(2,4)} & \mathbf{E}_m^{(3,4)} \\ \mathbf{0} & \mathbf{0} & \mathbf{F}_k^{(1,3)} & \mathbf{0} & \mathbf{F}_k^{(2,4)} & \mathbf{F}_m^{(3,4)} \end{bmatrix} \tag{21}$$

$$\boldsymbol{\Delta} = \begin{bmatrix} \boldsymbol{\Delta}_m^{(1,2)} \\ \boldsymbol{\Delta}_k^{(1,a)} \\ \boldsymbol{\Delta}_k^{(1,3)} \\ \boldsymbol{\Delta}_k^{(2,a)} \\ \boldsymbol{\Delta}_k^{(2,4)} \\ \boldsymbol{\Delta}_m^{(3,4)} \end{bmatrix} \tag{22}$$

$$\boldsymbol{\Phi} = \begin{bmatrix} \mathbf{0} \\ \boldsymbol{\Phi}_k^{(1,a)} \\ \boldsymbol{\Phi}_k^{(1,3)} \\ \boldsymbol{\Phi}_k^{(2,a)} \\ \boldsymbol{\Phi}_k^{(2,4)} \\ \boldsymbol{\Phi}_m^{(3,4)} \end{bmatrix} \tag{23}$$

The designation of the submatrices and the subvectors is given in Ref. [13].

Solving this system of linear equations makes it possible to find the weighting coefficients. The determined weighting coefficients are used to calculate the temperature distribution in the regions of the unit subdomain according to Eqs. (2)–(5).

4. Numerical results and discussion

The present method was applied to calculate the temperature distribution in the resistive thermal sensor based on a platinum thin film.

A polyimide foil was chosen as the substrate. The thickness of the substrate was 20 μm. The thermal conductivity of polyimide was equal to 0.148 $W \cdot m^{-1} \cdot K^{-1}$. The polyimide glue was used to fasten the sensor to the surface of an object. The thickness of the glue layer was chosen to be equal to 10 μm.

The meander structure of the sensor had the square shape with the following parameters. The width of the meander strip was equal to 10 μm. The distance between meander strips was equal to 10 μm. The form factor of the meander structure was chosen to be equal to 136. The resistance of the sensor was equal to 100 Ω at the temperature of 273.15 K. The temperature resistance coefficient of the platinum thin film was assumed to be 0.0034 K^{-1}.

The value of the measuring current was equal to 1 mA. The value of the convective heat transfer coefficient was chosen to be equal to 5.6 $W \cdot m^{-2} \cdot K^{-1}$. The temperatures of the ambient air and the surface temperature of the object under investigation were assumed to be 300 K and 400 K, respectively.

The overheating temperature distribution in the unit subdomain of the sensor with the above-mentioned parameters is presented in Fig. 3. The overheating temperature, ΔT, are determined concerning the surface temperature of the object as follows

$$\Delta T = T_j - T_s \tag{24}$$

The overheating temperature distribution along the upper boundary of the unit subdomain is shown in Fig. 4. This temperature distribution is important since the temperature on the section of the upper boundary (region 1) is assumed to be equal to the temperature of the meander strip. It is worthwhile to compare the temperature of the resistive layer (the meander strip) calculated by the present method with the value determined with the help of the lumped model based on the electro-thermal analogy. In the case of the lumped model, the overheating temperature of the resistive layer, ΔT_{lm}, is equal to

$$\Delta T_{lm} = \left[R_0 I^2 (1 - \alpha T_0) + 2hk_f b^2 T_a + 2k_f b^2 \lambda_s \lambda_c T_s / (d_s \lambda_c + d_c \lambda_s)\right] \times \left[-\alpha R_0 I^2 + 2hk_f b^2 + 2k_f b^2 \lambda_s \lambda_c / (d_s \lambda_c + d_c \lambda_s)\right]^{-1} - T_s \tag{25}$$

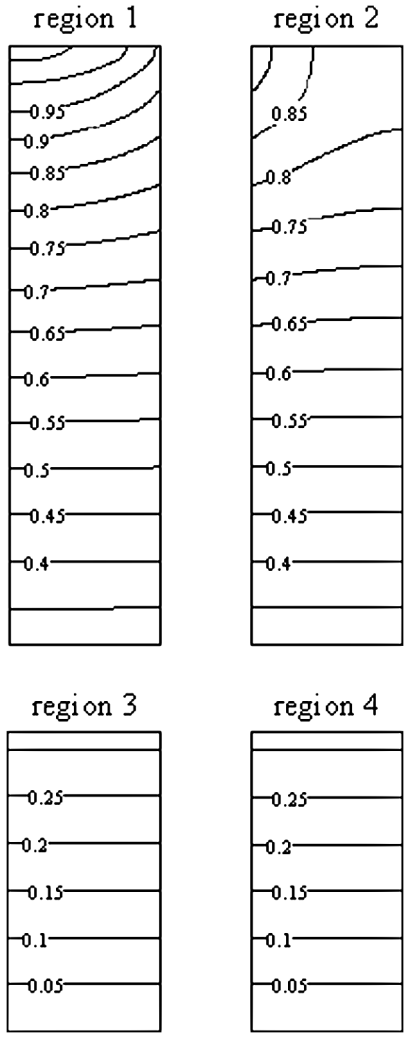

Fig. 3. Temperature distribution in the equivalent structure of the unit subdomain: overheating temperature maps of the regions plotted by isotherms.

For the chosen parameters of the sensor, the numerical value of the overheating temperature calculated with the lumped model is $\Delta T_{lm} = 0.954$ K. Comparing this value and data obtained with the present model (Figs. 3 and 4) one can see that the estimation of the overheating temperature with the help of the lumped model leads to the understated value.

The data of Figs. 3 and 4 indicate that the greatest value of the overheating temperature is observed in the left upper corner of the unit subdomain. This point corresponds to the centre of the meander strip. The value of the overheating temperature in this point can be used as the characteristic temperature to describe the absolute error of the sensor due to the self-heating. Therefore, below we consider the dependence of the overheating temperature in the centre of the meander strip, ΔT_{cm}, on the various parameters. During the calculation of the dependence on one parameter, the other parameters are assumed to be equal to the values defined above.

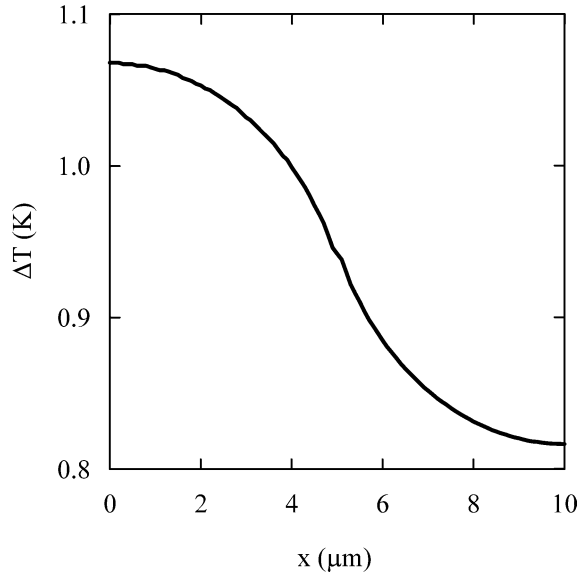

Fig. 4. Overheating temperature distribution along the upper boundary of the equivalent structure.

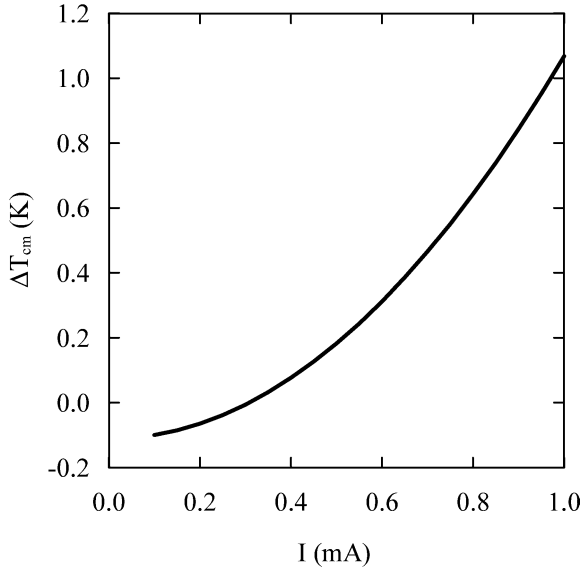

Fig. 5. Overheating temperature in the centre of the meander strip as a function of the measuring current.

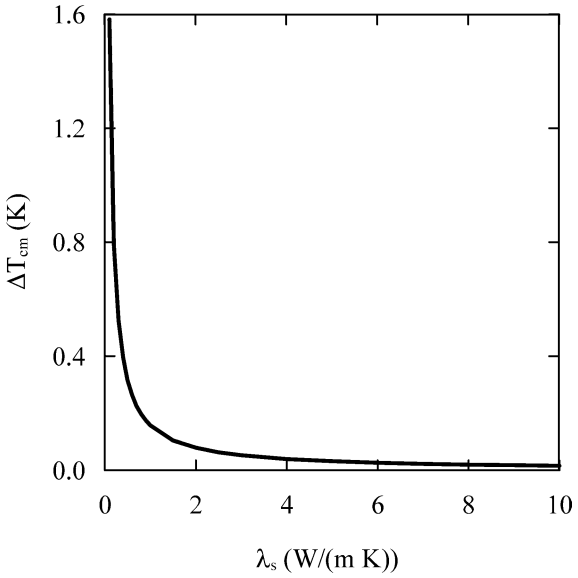

Fig. 6. Overheating temperature in the centre of the meander strip as a function of the thermal conductivity of the substrate.

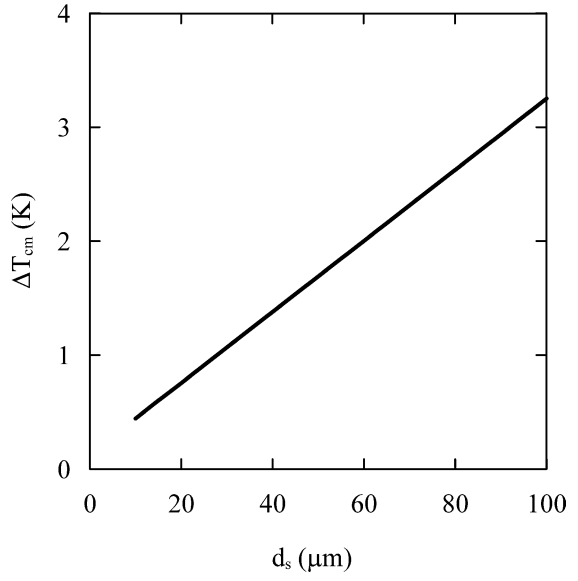

Fig. 7. Overheating temperature in the centre of the meander strip as a function of the thickness of the substrate.

The dependence of the overheating temperature in the centre of the meander strip on the measuring current is shown in Fig. 5. This dependence is like to the square law. For the small measuring currents, the overheating temperature is negative. This indicates that the convective heat transfer predominates over the heat transfer through the substrate and the connective layer by thermal conduction and the temperature in the centre of the meander strip becomes smaller than the surface temperature of the object.

Fig. 6 shows the dependence of the overheating temperature in the centre of the meander strip on the thermal conductivity of the substrate. The feature of this dependence is the drastic decrease of the overheating temperature with increasing the thermal conductivity of the substrate, for the small values of the thermal conductivity. The further increase of the thermal conductivity does not lead to the visible decrease of the overheating temperature. This feature must be taken into account in designing the resistive thin-film thermal sensor when we want to decrease the absolute error due to the self-heating by means of increasing the thermal conductivity of the substrate.

The dependence of the overheating temperature in the centre of the meander strip on the thickness of the substrate is shown in Fig. 7. The overheating temperature varies linearly with the thickness of the substrate.

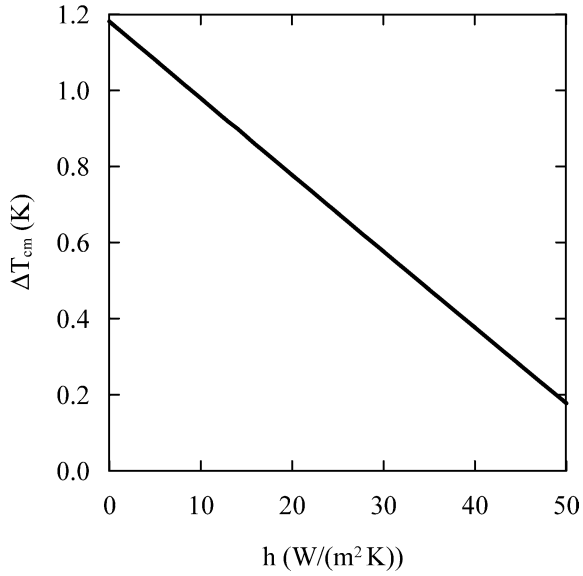

Fig. 8. Overheating temperature in the centre of the meander strip as a function of the convective heat transfer coefficient.

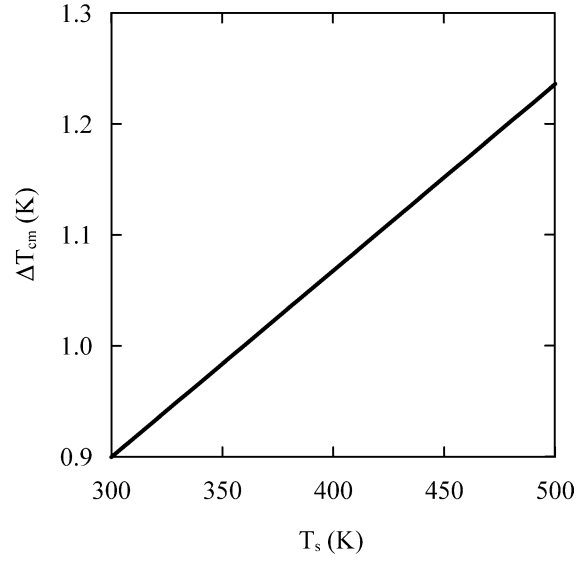

Fig. 9. Overheating temperature in the centre of the meander strip as a function of the surface temperature of the object under consideration.

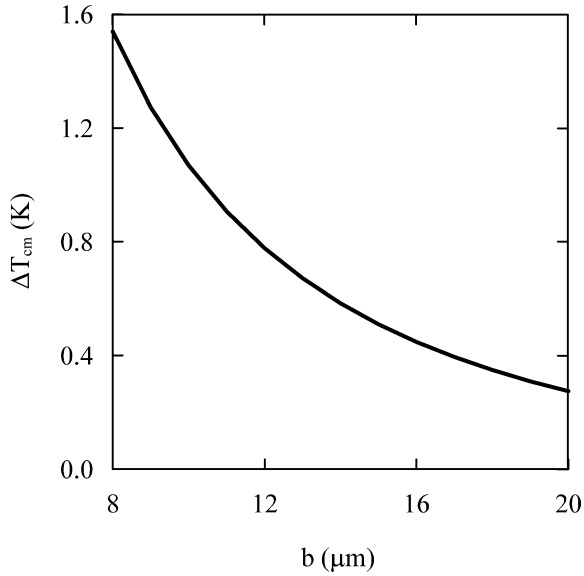

Fig. 10. Overheating temperature in the centre of the meander strip as a function of the width of the meander strip, $a = 10$ μm.

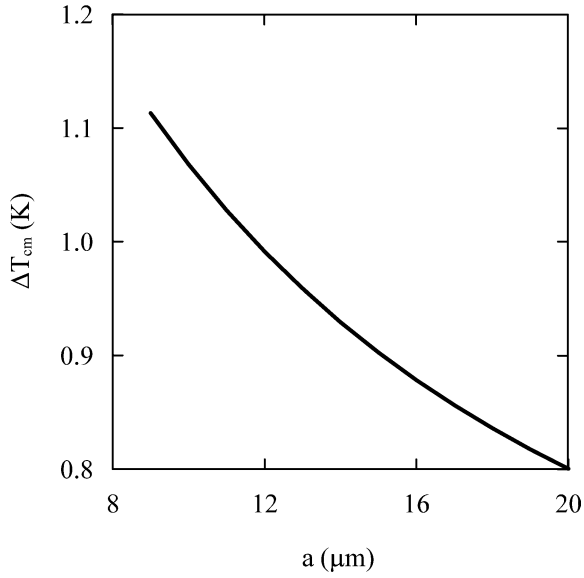

Fig. 11. Overheating temperature in the centre of the meander strip as a function of the distance between the meander strips, $b = 10$ μm.

Fig. 8 shows the dependence of the overheating temperature in the centre of the meander strip on the convective heat transfer coefficient. The overheating temperature decreases linearly with increasing the convective heat transfer coefficient. For large values of the convective heat transfer coefficient, the overheating temperature can be negative. In this case, the convection heat transfer predominates and the temperature in the centre of the meander strip is smaller than the surface temperature of the object.

The dependence of the overheating temperature in the centre of the meander strip on the surface temperature of the object under investigation is shown in Fig. 9. The overheating temperature varies linearly with increasing the surface temperature.

It is worthwhile to consider the dependencies of the overheating temperature in the centre of the meander strip on its construction parameters: the width of the meander strip, b, and the distance between the meander strips, a. These dependencies are shown in Figs. 10 and 11, respectively. As can be seen from these figures, the overheating temperature decreases with increasing a and b. The analysis of these dependencies indicates that the overheating temperature is more susceptible to the change of b than a, especially for the small values of these parameters. This feature must be taken into account in designing the resistive thin-film thermal sensor. To reduce the absolute error due to the self-heating and, respectively, the overheating temperature it is worthwhile to

increase the width of the meander strip than the distance between the strips.

5. Conclusion

In this paper, the method of modelling the temperature distribution in the resistive thin-film thermal sensors is presented. This method allows one to determine exactly the overheating temperature of the sensor and its absolute error due to the self-heating. The basic advantage of this method is the more accurate estimate of the sensor error due to the self-heating.

The present method can be useful in designing the resistive thin-film thermal sensors. With the help of this method, the design of the sensors can be optimized to minimize their absolute error due to the self-heating. In addition, this method can be applied to calculate the overheating temperature and the absolute error due to the self-heating in other types of resistive thin-film sensors (tensoresistive, photoresistive, and magnetoresistive sensors).

Our investigation and the present practical results show that this method can be used for creating CAD tools for the resistive thin-film thermal sensors. Its usage can be realized with the help of the common mathematical software.

References

[1] G.C.M. Meijer, A.W. van Herwaarden, Thermal Sensors, Institute of Physics Publishing, Bristol, 1994.

[2] G. Wiegleb, Sensortechnik. Übersicht, Applikation, Anwendungen, Franzis, München, 1986.

[3] G. Asch, P. Desgoutte, P. André, et al., Les capteurs en instrumentation industrielle, Bordas, Paris, 1991.

[4] V. d'Alessandro, N. Rinaldi, A critical review of thermal models for electro-thermal simulation, Solid-State Electronics 46 (2002) 487–496.

[5] S.B. Crary, Thermal management of integrated microsensors, Sensors and Actuators 12 (1987) 303–312.

[6] S.B. Crary, The finite-element method for microsensors, J. Electrochem. Soc. 134 (1987) 2937–2940.

[7] A.U. Dillner, E. Kessler, S. Poser, V. Baier, J. Müller, Low power consumption thermal gas-flow sensor based on thermopiles of highly effective thermoelectric materials, Sensors and Actuators A 60 (1997) 1–4.

[8] J.-B. Lee, I.-S. Kim, Y.-C. Sim, T.-Y. Kim, Optimization and fabrication of a dual thermopile sensor based on the BEM, Sensors and Actuators A 64 (1998) 179–184.

[9] S.D. Kolev, M. Ádám, C. Dücsö, I. Bársony, C. Cobianu, A. Van den Berg, Thermal modelling of a porous silicon-based pellistor-type catalytic flammable gas sensor with two supporting beams, Microelectronics J. 31 (2000) 339–342.

[10] http://www.honeywell-sensor.com.cn/prodinfo/sensor_temperature/technical/c15_141.pdf.

[11] A.D. Kokkas, Thermal analysis of multiple-layer structures, IEEE Trans. Electron Devices ED-21 (1974) 674–681.

[12] A. Csendes, V. Székely, M. Rencz, An efficient thermal simulation tool for ICs, microsystem elements and MCMs: the μS-THERMANAL, Microelectronics J. 29 (1998) 241–255.

[13] A.G. Kozlov, Analytical modelling of steady-state temperature distribution in thermal microsensors using Fourier method: Part 1. Theory, Sensors and Actuators A 101 (2002) 283–298.

[14] A.G. Kozlov, Analytical modelling of steady-state temperature distribution in thermal microsensors using Fourier method: Part 2. Practical application, Sensors and Actuators A 101 (2002) 299–310.